



Effect of temperature on the microwave absorbing properties of SiO₂/CNTs composite

Xiaofeng Li¹, Gang Fang¹, Kangsen Peng¹, and Guoyue Xu^{1,*}

¹ College of Materials Science and Technology, Nanjing University of Aeronautics and Astronautics, Nanjing 210016, China

Received: 18 November 2020

Accepted: 20 February 2021

Published online:
8 March 2021

© The Author(s), under exclusive licence to Springer Science+Business Media, LLC, part of Springer Nature 2021

ABSTRACT

In this work, SiO₂/CNTs nano-composites were synthesized by the modified Stöber method for exploring the microwave absorbing performance at gradient temperatures. The SEM results show that the as-prepared SiO₂ particles have spherical morphology, with a diameter of 100 nm, and the carbon nanotubes in the powder are interlaced. With increasing temperature, more and more SiO₂ spheres were seen to attach to the carbon nanotubes, and the increase in conductivity was ascribed to the increase in carrier concentration. Ascribed to the enhanced conductivity and the increasing interface between the SiO₂ particles and the carbon nanotubes, the real and imaginary parts of the complex permittivity were seen to gradually increase, contributing to the improving attenuation. Hence, the sample tested at 400 °C exhibited optimal microwave absorbing performance with a minimum reflection loss (RL) of − 9.76 dB and a bandwidth (RL < − 4 dB) of 4.1 GHz at a thickness of 2 mm, which basically covers the entire 8.2–12.4 GHz (X-band).

1 Introduction

In recent years, there has been growing interest of microwave. Meikap et al. [1–6] systematically studied the influence of microwave pretreatment on the rheological properties of coal-water slurries. And in the field of electromagnetic (EM) absorption, research on microwave absorbing materials (MAM) has mainly focused on room temperature materials [7], while little research has been done in the field of medium and high temperatures. Generally, MAMs at medium and high temperature include materials based on carbon, SiC, and ceramic. Wen et al. [8] fabricated SiO₂/CNTs composites by mechanical mixing, which

showed non-ideal microwave absorption performance (RL < − 5 dB) at low-carbon nanotube filling rate and low thickness at 400 °C. Mu et al. [9–11] systematically studied the wave absorbing performance of SiC_f/SiC composites with different fillers at X-band and 400 °C. A reflection loss of SiC_f fabric samples, which exhibits an absorption bandwidth of 8.2–12.4 GHz (RL < − 8 dB) at a thickness of 3.4 mm, was observed. A composite material based on Ti₃SiC₂ was prepared by Liu et al. [12] through a hot-pressing sintering method. The material showed a minimum RL of − 12 dB and a bandwidth of about 2 GHz at 400 °C. The conductivities of these above-mentioned materials are so low at 400 °C that they

Address correspondence to E-mail: xuguoy@nuaa.edu.cn

cannot provide sufficient conductivity loss, which contributes to enhancing the microwave absorbing performance. The performance is not ideal under low thickness conditions, and the preparation process is relatively complicated.

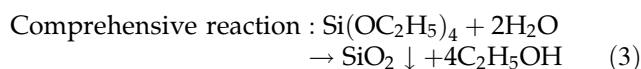
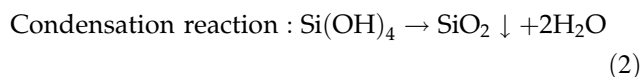
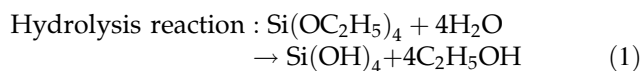
Carbon materials mainly include carbon black, carbon nanotubes (CNTs), and graphene, which have the advantages of high conductivity, perfect quantum tunneling effect, large specific surface area, low density, and excellent temperature resistance. Although carbon materials possess high conductivity loss performance, the high value of the real part of the permittivity results in poor impedance matching [12] with the free space. This is because a large number of electromagnetic waves are reflected from the surface of the material due to the skin effect. Therefore, carbon materials are usually composited with low-permittivity materials or magnetic materials to reduce the real part of the permittivity and improve the impedance matching. In addition, the imaginary part of the complex permittivity represents the ability to attenuate electromagnetic waves. Researchers generally rely on polarization relaxation phenomena to increase the imaginary part of the dielectric of the sample to enhance the absorption of electromagnetic waves. SiO₂ is an ideal wave-transparent material which possesses good chemical stability, high-temperature resistance, and excellent electrical insulation properties. Therefore, SiO₂ can be used as a candidate material for improving the impedance matching of carbon materials, and can also be used at medium and high temperatures due to its excellent high-temperature stability.

Hence, in this work, we used the modified Stöber method [13] to grow SiO₂ pellets on carbon nanotubes in situ, to form SiO₂/CNTs composite materials. Polarization relaxation and electronic conductivity from the CNTs contributes to the dielectric loss, while the attached SiO₂ can also enhance the interfacial polarization loss as well as the impedance matching. Finally, the sample testing at 400 °C shows optimal microwave absorbing properties with absorption bandwidth of 4.1 GHz over X-band (RL < − 4 dB) at a thickness of 2.05 mm and the best RL_{min} values of − 9.76 dB at a thickness of 2.4 mm.

2 Experimental procedure

The SiO₂/CNTs nano-composites were synthesized by the modified Stöber method and the schematic as shown in Fig. 1. In a beaker, 200 mL ethanol, 20 mL TEOS, 10 mL deionized water, and 9 mL ammonia were added, to which a mass fraction of 1% of acidified carbon nanotubes was added. Then, the obtained mixture was placed in a water bath at 40 °C and magnetically stirred at a speed of 220 r/min for 6 h. After the hydrothermal reaction, the precipitate was collected by centrifugation, washed with deionized water and ethyl alcohol three times, and then dried in an oven at 60 °C for 24 h. At last, the as-dried SiO₂/CNTs powders, containing a binder of sodium silicate aqueous, were pressed to obtain samples of 22.86 mm (length) × 10.16 mm (width) × 4.32 mm (thickness), named SCNT. Vector network analyzer (VAN) was used to investigate microwave absorbing properties of the SCNT at X-band, a heating furnace and a circulating cooling water tank were used to heat the sample and cool VAN respectively. The heating process is to heat the sample at 5 °C/min and the temperature is kept at the test temperature (100 °C, 200 °C, 300 °C, 400 °C) for 10 min, then cooled to room temperature.

The reaction equation for preparing SiO₂ by the Stöber method is shown as follows:



The morphology of the sample was observed by scanning electron microscopy (S-3400 N, Hitachi, Japan). An X-ray diffractometer (Cu K α radiation, Advanced D8, Bruker) was involved in identifying the phases of the samples. Raman spectra were obtained from a Lab RAM HR800 spectrometer (Jobin–Yvon, Longjumeau, France). A resistivity measuring instrument (FT-351) and a high-temperature test box were combined to test the resistivity of the absorbent. The electromagnetic parameters of the samples, at different test temperatures, in the X-band, were measured through the network analyzer (Agilent, N5244A, America), and the reflection loss was

calculated according to the transmission line theory (Fig. 1).

3 Results and discussion

The SEM micrographs of the SCNT samples are shown in Fig. 2. It can be observed that SiO₂ and CNTs are well mixed (as shown in Fig. 2a and b). The SiO₂ pellets are unbroken and uniform in size, with a diameter about 100 nm. The carbon nanotubes are dendritic, with a particle size equivalent to that of the SiO₂ pellets. Figure 2c and d are the high-magnification images of Fig. 2a and b, respectively. In order to improve the nucleation rate of silicon balls on the carbon nanotubes, the carbon nanotubes were artificially acidified to obtain surface defects. As we expected, a part of the SiO₂ particles had grown on the CNTs.

Figure 3 presents the XRD pattern of the SCNT sample. The XRD pattern shows that there is a unique dispersion peak at 20°–30°, indicating that the synthesized SiO₂ particles have an amorphous structure. However, the characteristic peaks of carbon nanotubes near 26° were obscured by the dispersion peaks.

In order to further analyze the structure of carbon tubes, the Raman spectrum of the SCNT sample was tested at 400 °C, as shown in Fig. 4. The peaks at 1350 cm⁻¹ and 1580 cm⁻¹ correspond to the peak D and peak G of the carbon material, respectively. The peak D represents amorphous carbon or graphite with defects, and the peak G is derived from graphitized carbon with good symmetry and order in the sample. The ratio of the peak intensities of peaks D and G, namely I_D/I_G, is usually used to represent the degree of graphitization of carbon-based materials. The ratio

of the SCNT sample is 0.574, indicating that the carbon nanotubes have a higher degree of graphitization.

Figure 5 shows the real part of the complex permittivity (ε') and the imaginary part of the complex permittivity (ε'') of the SCNT sample at different test temperatures. It can be seen from Fig. 5a that as the test temperature increases, the complex permittivity gradually increases. The ε' reaches a minimum value and is only 6.4–5.25 in the range of 8.2–10.4 GHz when the test temperature was 25 °C. As the test temperature rose to 400 °C, ε' reached the maximum value with 14.8–11.8 in the X-band. Similarly, it can be found from Fig. 5b that ε'' was lowest at 25 °C, *i.e.*, 1.0–0.6 at 400 °C, the value of imaginary parts of the complex permittivity could reach a value of 2.6.

The trend of complex permittivity can be explained by the Debye theory, which usually demonstrates the process of the absorber interacting with the electromagnetic field and judges the polarization category of the materials. The complex permittivity can be expressed by the following equations [14, 15]:

$$\epsilon' = \epsilon_{\infty} + \frac{\epsilon_s - \epsilon_{\infty}}{1 + (2\pi f)^2 \tau^2} \quad (4)$$

$$\epsilon''_{relax} = \frac{2\pi f \tau (\epsilon_s - \epsilon_{\infty})}{1 + (2\pi f)^2 \tau^2} \quad (5)$$

$$\epsilon''_{\sigma} = \frac{1}{2\pi \rho f} \quad (6)$$

$$\epsilon'' = \epsilon''_{relax} + \epsilon''_{\sigma} = \frac{2\pi f \tau (\epsilon_s - \epsilon_{\infty})}{1 + (2\pi f)^2 \tau^2} + \frac{1}{2\pi \rho f} \quad (7)$$

where ε_s, ε_∞, f, and ρ represent the static permittivity, high-frequency permittivity, frequency, and resistivity, respectively. τ is the relaxation time related to

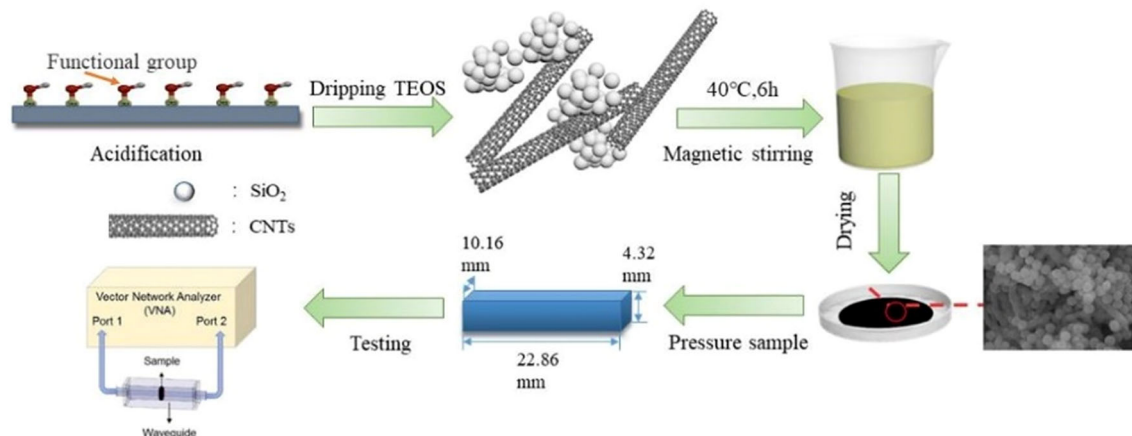


Fig. 1 SiO₂/CNTs sample preparation flow chart

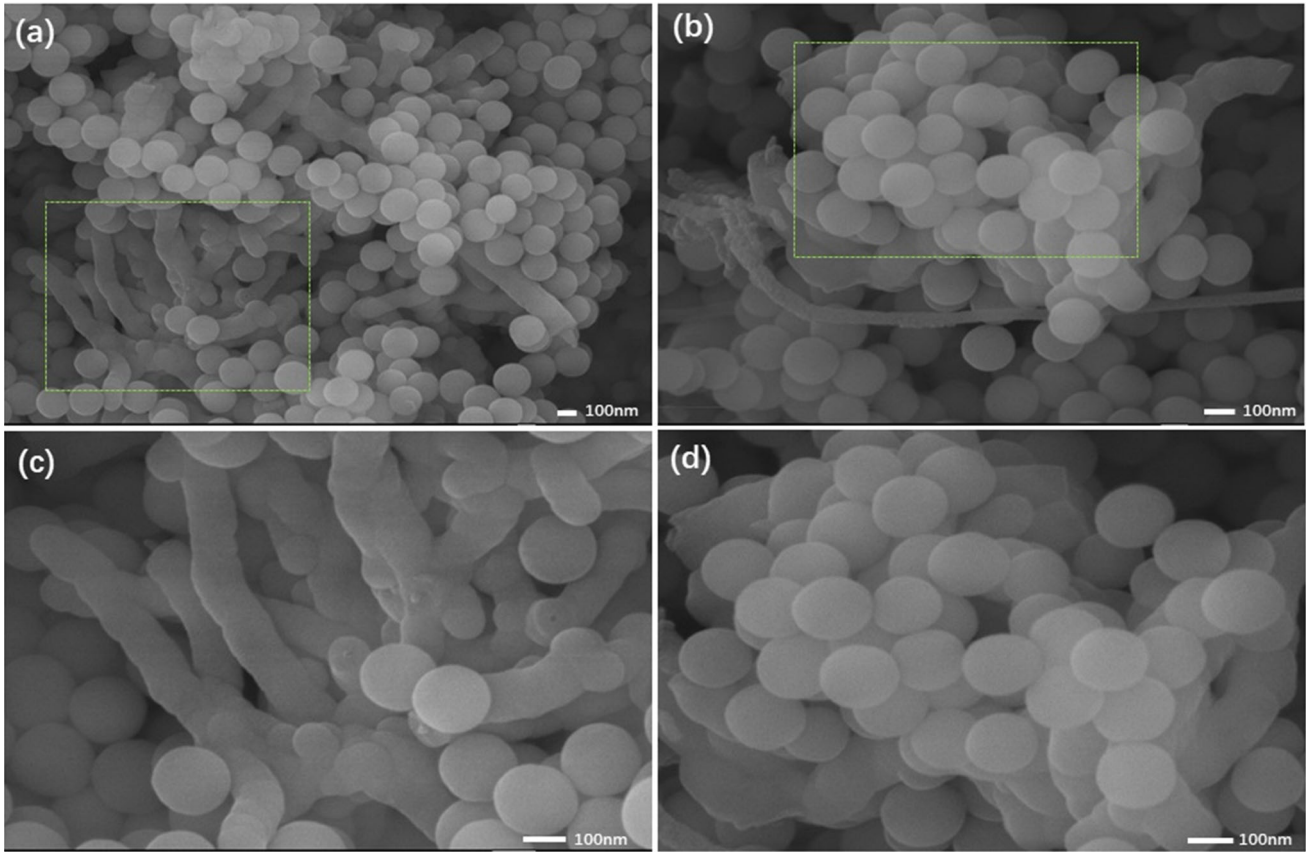


Fig. 2 a, b SEM images of the SCNT powder samples and c, d the corresponding high-magnification images

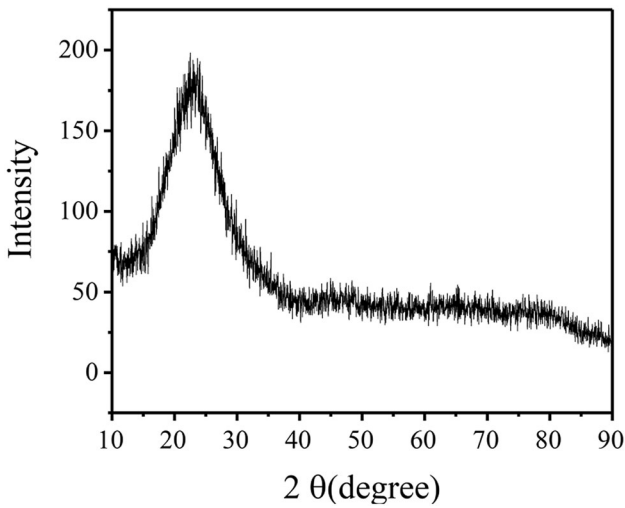


Fig. 3 XRD pattern of SCNT sample

temperature [16], $\sigma(T)$ is the conductivity related to temperature T , which can be written as follows:

$$\tau = \frac{1}{2\nu} e^{\frac{E}{kT}} \tag{8}$$

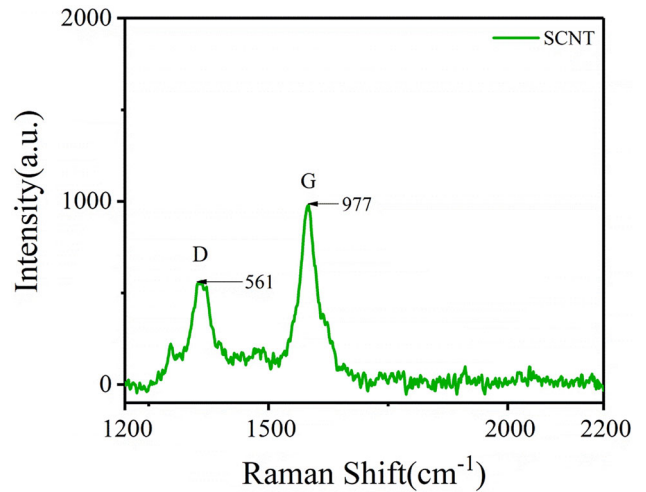


Fig. 4 Raman spectrum of SCNT

$$\sigma = \sigma_0 \exp\left(\frac{-E}{KT}\right) \tag{9}$$

In the above two equations, E is the activation energy, k is the Boltzmann constant, ν is the frequency of the

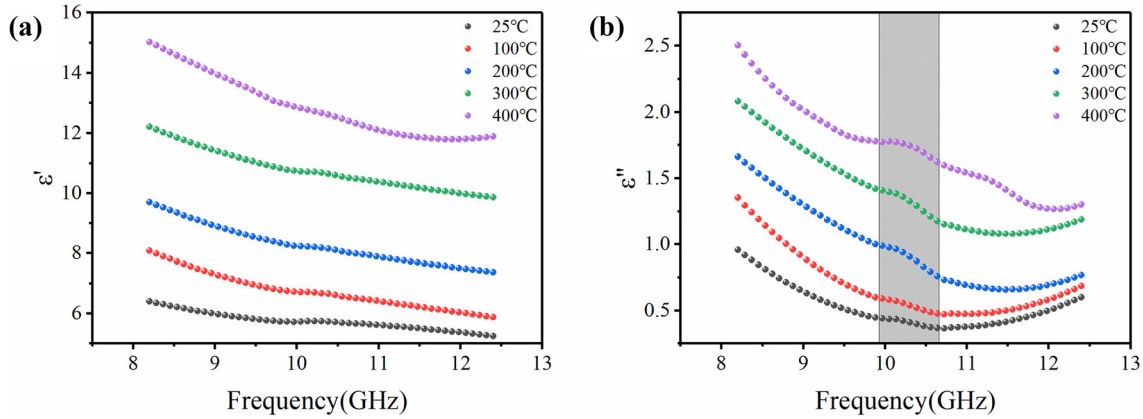


Fig. 5 **a** The real part of complex permittivity and **b** the imaginary part of complex permittivity of SCNT samples at different test temperatures

lattice vibration, T is the absolute temperature, and σ_0 is the pre-referential factor.

According to Eq. (4), the real part of the complex permittivity is inversely proportional to the relaxation time τ , causing an increase of ϵ' . And according to Eq. (5), as the temperature increases, the relaxation time τ decreases, polarization no longer lags behind the change of electric field and can be established completely, which increases the polarization loss of the material, causing an increase of ϵ_{relax}'' . Figure 6 shows the change in resistivity of the sample at different test temperatures, which can be verified by the Arrhenius relationship between conductivity and temperature in Eq. (9). It is known the carrier is sensitive to the temperature and the intrinsic carrier concentration would increase when the temperature rises, contributing to the enhanced conductivity. So conductivity loss (ϵ_{σ}'') would also improve based on the Eq. (6) [17]. The ϵ'' is determined by both the ϵ_{σ}'' and ϵ_{relax}'' , as shown in Eq. (7). As the test temperature increases, the ϵ_{σ}'' and ϵ_{relax}'' both increase, and so does the ϵ'' . To sum up, the real and imaginary parts of the complex permittivity increase with the increase of the test temperature.

Therefore, the leading factor for the increase of the ϵ'' in Fig. 5b is that the conductivity loss, ϵ_{σ}'' , increases with the increase of temperature, and the polarization loss, ϵ_{relax}'' , demonstrates the relaxation peak at the shaded part of Fig. 5b.

Based on Eqs. (4 and 5) we can obtain Eq. (10):

$$\left(\epsilon'' - \frac{\epsilon_s + \epsilon_{\infty}}{2}\right)^2 + (\epsilon'')^2 = \left(\frac{\epsilon_s - \epsilon_{\infty}}{2}\right)^2 \tag{10}$$

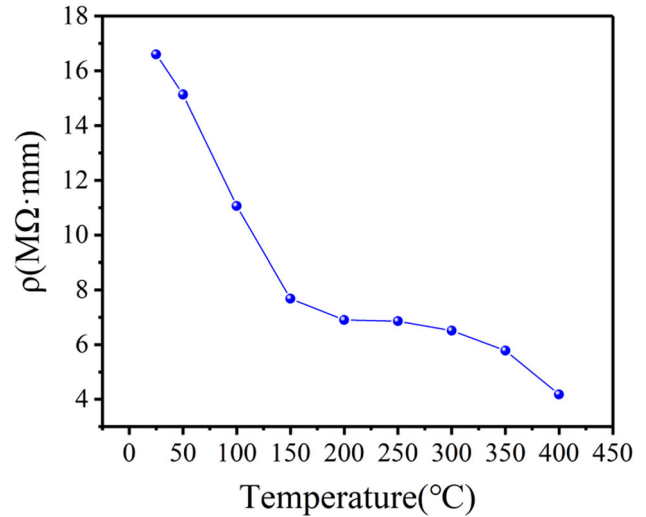


Fig. 6 Resistivity of SCNT sample as a function of temperature

Figure 7 shows a Cole–Cole curve with the ϵ' as the x -axis and the ϵ'' as the y -axis. If the relaxation polarization phenomenon occurs, it can be observed in the Cole–Cole curve, where each semicircle corresponds to a polarization process [18]. It can be seen from Fig. 7a–e that a semicircle appears in all samples, which represents a polarization process, while the straight line represents the conductivity loss [19]. Generally speaking, in the range of 2–18 GHz, the polarization mode of the sample generally includes ion displacement polarization, electron displacement polarization, and interface polarization [20]. Different polarization modes correspond to different relaxation times, and the polarization effect will only occur if the frequency reciprocal is greater than the relaxation time. The interface polarization takes a long time,

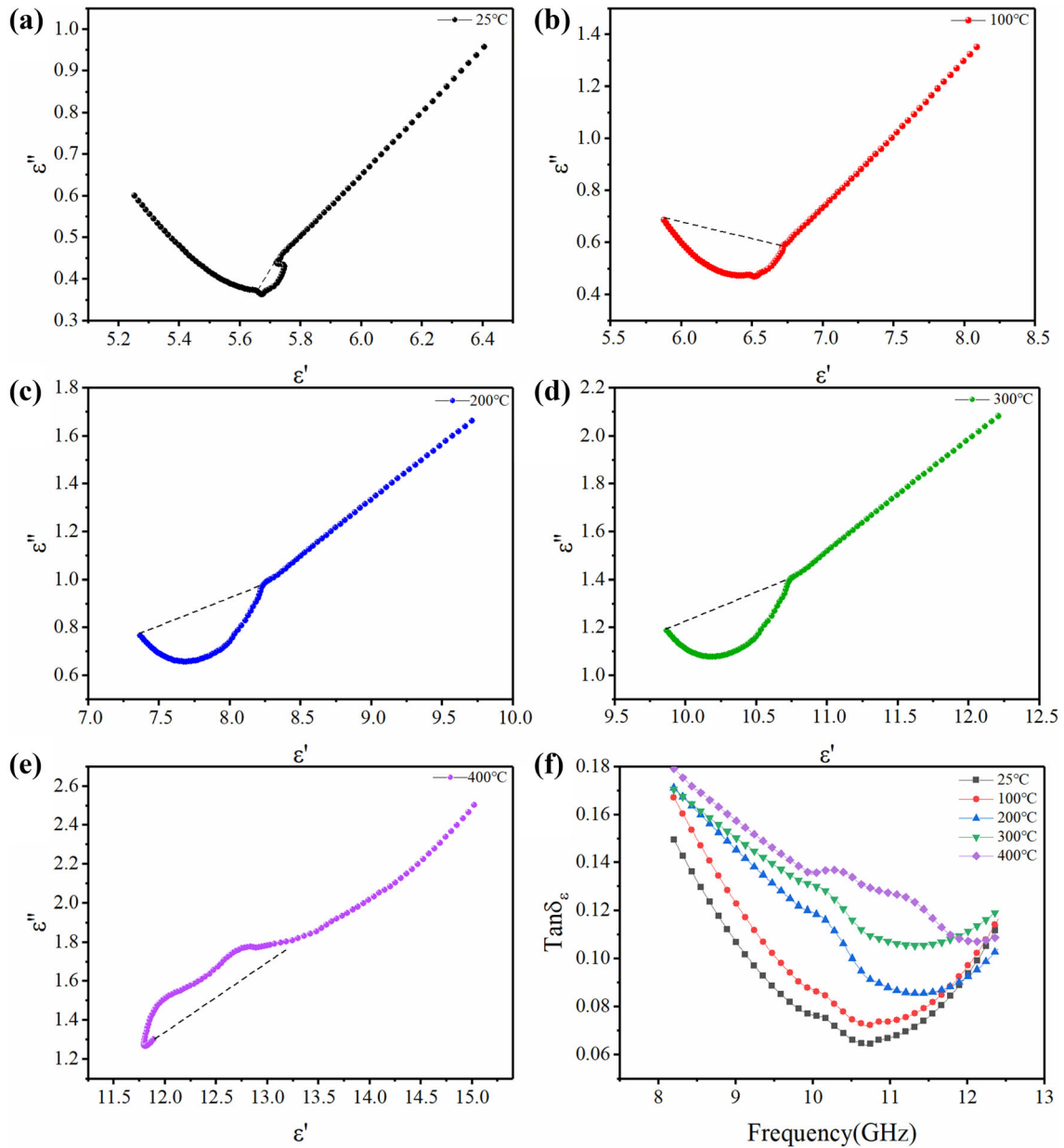


Fig. 7 The ϵ'' – ϵ' curve of SCNT material at different test temperatures: **a** 25 °C, **b** 100 °C, **c** 200 °C, **d** 300 °C, **e** 400 °C, and **f** the dielectric loss tangent

generally in the range of 10^{-10} – 10^{-2} s and the reciprocal of interface relaxation time is found to be comparable to the relaxation peak at 10.5 GHz. Based on Eqs. (5) and (8), it can be seen that as the temperature increases, the relaxation time decreases, and the interface polarization loss of the sample increases slightly; thus, as the temperature increases, the higher relaxation peak. Figure 7f shows the dielectric loss tangent ($\tan \delta_e$) curves which have been

calculated from ϵ''/ϵ' . The higher is the value of $\tan \delta_e$, the stronger is the dielectric loss ability of the material to electromagnetic waves. It can be seen from the Fig. 7f that the sample tested at 400 °C shows the optimal microwave absorbing performance.

It is known that the microwave absorbing properties of materials are determined by attenuation characteristics (α) and impedance matching, which can be calculated by the following equations [21, 22]:

$$\alpha = \frac{\sqrt{2}\pi f}{c} \times \sqrt{(\mu''\epsilon'' - \mu'\epsilon') + \sqrt{(\mu''\epsilon'' - \mu'\epsilon')^2 + (\mu'\epsilon'' + \mu''\epsilon')^2}} \quad (11)$$

$$|Z_m/Z_0| = \left| \sqrt{\frac{\mu_r}{\epsilon_r}} \right| \quad (12)$$

where f defined as the frequency, c the speed of light, and Z_m ($Z_m = \sqrt{\mu_r\mu_0/\epsilon_r\epsilon_0}$) is the wave impedance of the medium. The sample in this work is non-magnetic, so $\mu' = 1$ and $\mu'' = 0$ in the Eq. (9). The closer the value of $|Z_m / Z_0|$ is to 1, the better are the impedance matching characteristics.

Figure 8 illustrates the attenuation characteristics and impedance matching of the SCNT sample. It can be seen from Fig. 8a that the as-prepared sample has the largest attenuation constant at 400 °C, which is attributed to the highest dielectric loss at 400 °C. The peaks around 10.5 GHz, at different test temperatures, are caused by the interface polarization loss described above.

It can be observed from Fig. 8b that the impedance matching of the sample is the best at 25 °C and the worst at 400 °C. The above analysis indicates that the complex permittivity of the sample increases as the test temperature rises due to the enhanced conductivity. The higher conductivity would generate current under the incidence of electromagnetic waves on to the surface of a material due to the skin-effect; thus, a large number of electromagnetic waves cannot enter the absorbent and be reflected, which will make the impedance matching characteristics worse [23].

The reflection loss graphs of the SCNT samples at different test temperatures are shown in Fig. 9. The absorption peaks of the SCNT samples at different test temperatures are all at 8.2 GHz. As the test temperature increases, the minimum RL value of the sample gradually decreases, and the loss capability gradually increases. When the test temperature is 400 °C, the reflection loss of the sample reaches the highest value, and the absorption bandwidth is also significantly broadened. Furthermore, at 25 °C, an absorption peak appears for the sample with a thickness of about 4 mm, while at 400 °C, the sample with a thickness of 2.4 mm has good absorption performance. The electromagnetic microwave absorption performance of the sample is characterized by calculating the reflection loss. According to the transmission line theory, the electromagnetic wave reflection loss equations are as follows [24, 25]:

$$RL = 20 \log \left| \frac{Z_{in} - Z_0}{Z_{in} + Z_0} \right| \quad (13)$$

$$Z_{in} = Z_0 \sqrt{\frac{\mu_r}{\epsilon_r}} \tan \left[j \frac{2\pi f d}{c} \sqrt{\mu_r \epsilon_r} \right] \quad (14)$$

where Z_{in} is defined as the input impedance of the absorber, Z_0 is the impedance of free space, c is the speed of light, ϵ_r is the complex permittivity, and μ_r is the complex permeability.

When the test temperature of SiO₂/CNTs composites is 400 °C, the impedance matching is poor while the attenuation constant is the largest. It is generally believed that the attenuation constant plays a greater role in the absorption performance of the sample at a low thickness [25]. Therefore, the reflection loss of the sample to electromagnetic waves is

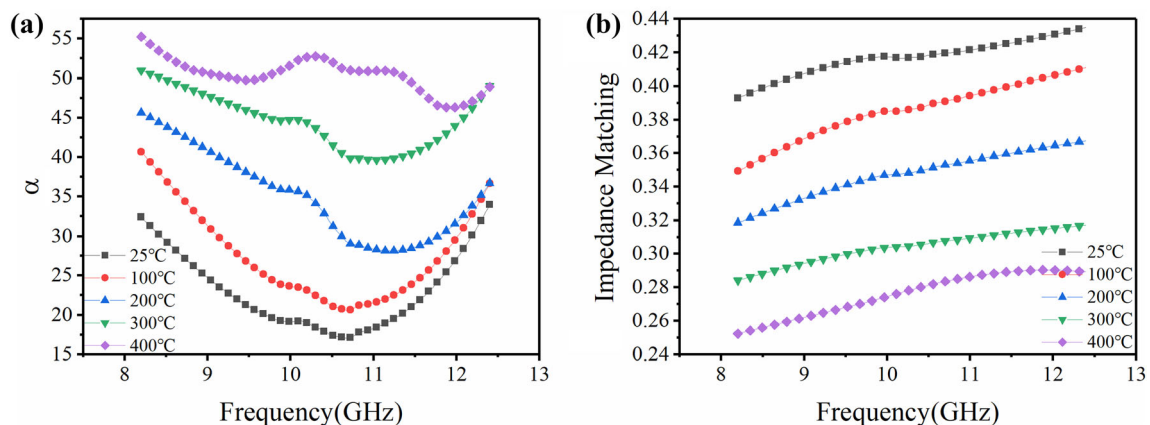


Fig. 8 **a** Attenuation constant and **b** impedance matching as a function of frequency, for SCNT at different test temperatures

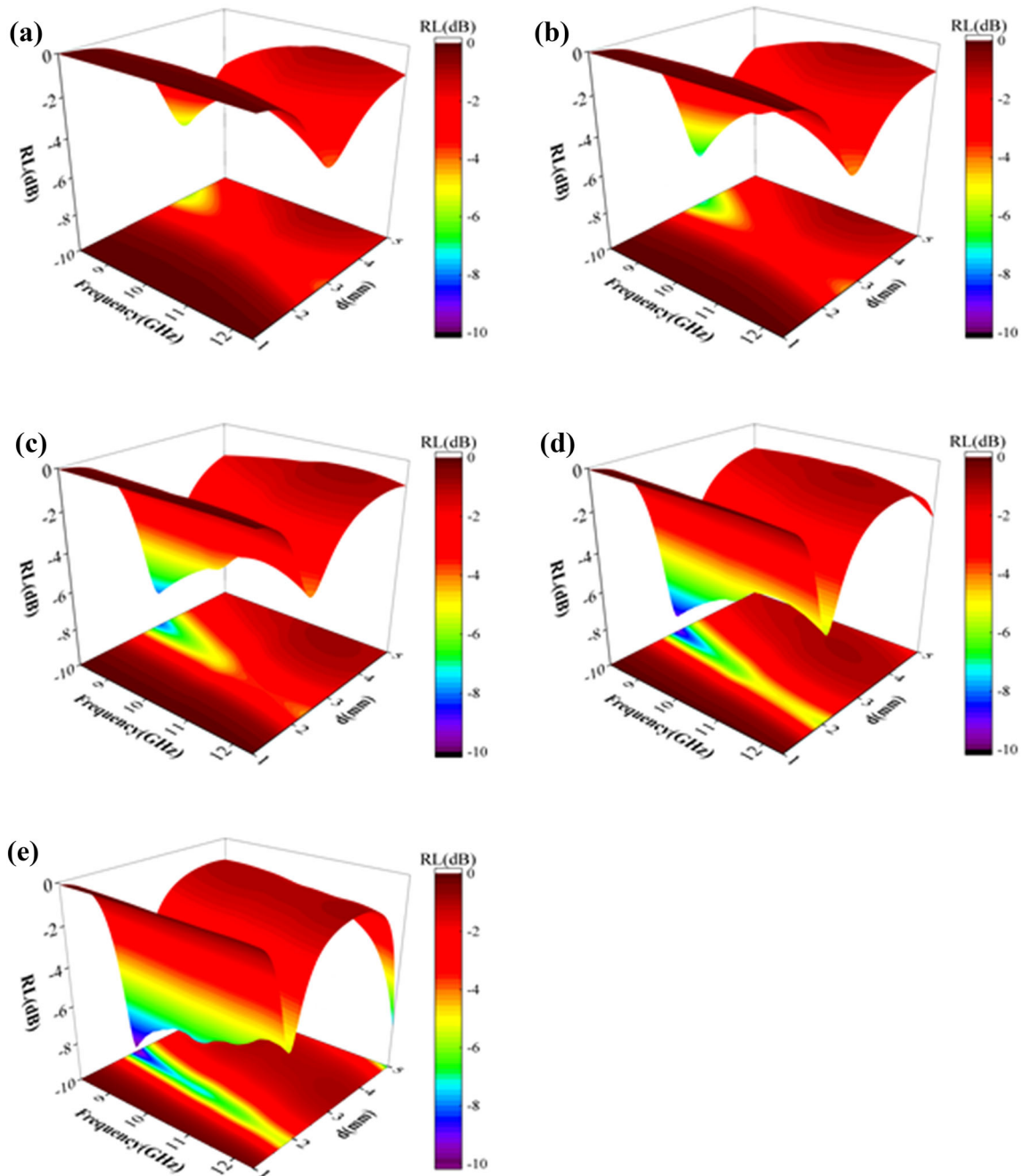


Fig. 9 Reflection loss graphs of SCNT samples at different test temperatures **a** 25 °C, **b** 100 °C, **c** 200 °C, **d** 300 °C, and **e** 400 °C

still better than other test temperatures, and the absorbing performance is greater at low thickness.

Figure 10 represents the maximum bandwidth and RL_{min} of the sample at the optimal matching-thickness of various test temperatures. As shown in Fig. 10a, with -4 dB as the benchmark, the sample tested at 400 °C reaches a maximum bandwidth of 4.1 GHz at a thickness of 2.05 mm, covering almost

the entire X-band, and the minimum RL value is -7.1 dB. At 400 °C, the thickness of the SCNT sample is 2.4 mm, the minimum RL value is -9.76 dB, and the maximum absorption bandwidth is 2.49 GHz. Its comprehensive absorption performance was still better than other test temperatures. In summary, the SCNT sample performs best at 400 °C.

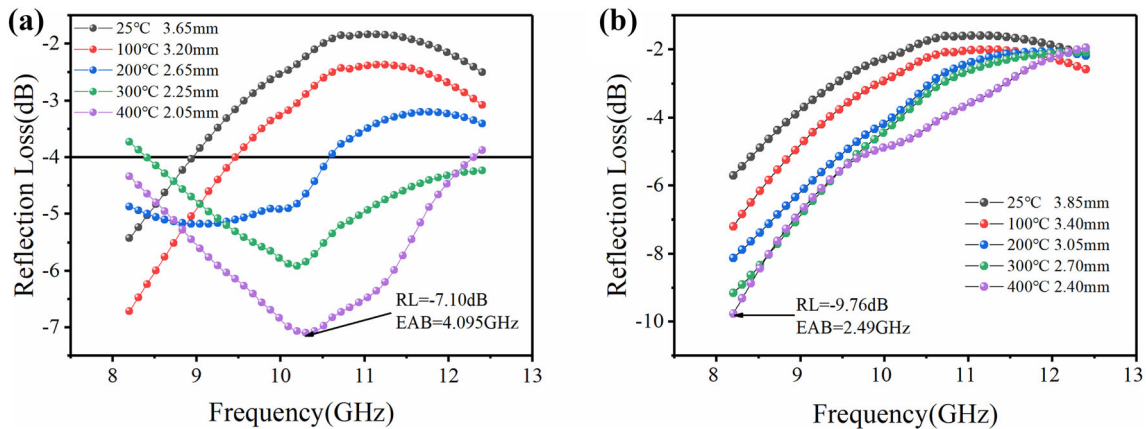


Fig. 10 Reflection loss graphs showing the **a** maximum bandwidth, **b** minimum RL of SCNT samples at different test temperatures

4 Conclusion

In this work, the SiO₂/CNTs composites were synthesized by the improved Stöber method. The average particle size of amorphous SiO₂ was 100 nm, and the SiO₂ spheres were attached to the CNTs. The ID/IG ratio was 0.574, indicating a high degree of graphitization of carbon nanotubes. With test temperature rising, the conductivity of the as-prepared sample increased due to the enhanced electrical activity. Moreover, the complex permittivity increased with the increase in the test temperature, which is ascribed to the increase in conductivity. Finally, due to the excellent dielectric loss, the sample testing at 400 °C showed optimal microwave absorbing properties with absorption bandwidth of 4.1 GHz over the X-band (RL < − 4 dB) at a thickness of 2.05 mm and the best RL_{min} values of − 9.76 dB at a thickness of 2.4 mm.

References

- B.K. Sahoo, S. De, M. Carsky, B.C. Meikap, *I&ECR* **49**(6), 3015–3021 (2010)
- B.K. Sahoo, S. De, B.C. Meikap, *J. Ind. Eng. Chem.* **25**, 122–130 (2015)
- B.K. Sahoo, S. De, B.C. Meikap, *J. Min. Sci. Technol.* **27**, 379–386 (2017)
- B.C. Meikap, N.K. Purohit, V. Mahadevan, *J. Coll. Interface Sci.* **281**(1), 225–235 (2005)
- B.K. Sahoo, S. De, M. Carsky, B.C. Meikap, *J. Ind. Eng. Chem.* **17**(1), 62–70 (2011)
- B.K. Sahoo, T.K. Das, A. Gupta, S. De, M. Carsky, B.C. Meikap, *S. Afr. J. Chem. Eng.* **23**, 81–90 (2017)
- X. Liu, Y.L. Qiu, Y.T. Ma, H.F. Zheng, L.S. Wang, Q.F. Zhang, Y.Z. Chen, D.L. Peng, *J. Alloys Compd.* **721**, 411–418 (2017)
- B. Wen, M.S. Cao, Z.L. Hou, W.L. Song, L. Zhang, M.M. Lu, H.B. Jin, X.Y. Fang, W.Z. Wang, J. Yuan, *Carbon* **65**, 124–139 (2013)
- Y. Mu, W.C. Zhou, Y. Hu, H.Y. Wang, F. Luo, D.H. Ding, Y.C. Qing, *Eur. Ceram. Soc.* **35**(11), 2991–3003 (2015)
- Y. Mu, W.C. Zhou, F. Wan, D.H. Ding, Y. Hu, F. Luo, *Compos. A* **77**, 195–203 (2015)
- Y.C. Qing, D.H. Ding, F. Luo, Y. Mu, W.C. Zhou, *J. Alloys Compd.* **637**, 261–266 (2015)
- Y. Liu, F. Luo, J.B. Su, W.C. Zhou, D.M. Zhu, *J. Alloys Compd.* **632**, 623–628 (2015)
- W. Stöber, A. Fink, E. Bohn, *J. Coll. Interface Sci.* **26**, 62–69 (1968)
- G.Z. Wang, Z. Gao, G.P. Wan, S.W. Lin, P. Yang, Y. Qin, *Nano Res.* **7**(5), 704 (2014)
- C.Y. Liu, Y.J. Zhang, J.G. Jia, Q. Sui, N. Ma, P.Y. Du, *Sci. Rep.* **5**, 9498 (2015)
- B.Y. Kuang, Y.K. Dou, Z.H. Wang, M.Q. Ning, H.B. Jin, D.Y. Guo, M.S. Gao, X.Y. Fang, Y.J. Zhao, J.B. Li, *Appl. Surf. Sci.* **445**, 383–390 (2018)
- W.L. Song, M.S. Cao, Z.L. Hou, X.Y. Fang, J. Yuan, *Appl. Phys. Lett.* **94**(23), 033105 (2009)
- X.Q. Cui, X.H. Liang, W. Liu, W.H. Gu, Y.W. Du, *Chem. Eng. J.* **381**, 122589 (2020)
- M.M. Lu, W.Q. Cao, H.L. Shi, X.Y. Fang, J. Yang, Z.L. Hou, H.B. Jin, W.Z. Wang, J. Yuan, M.S. Cao, *Mater. Chem. A* **2**, 10540 (2014)
- G. Fang, C.Y. Liu, G.Y. Xu, A.D. Xiao, K.S. Peng, Y.T. Zhang, Y.J. Zhang, *J. Alloys Compd.* **790**, 316–325 (2019)

21. J. Huo, L. Wang, H.J. Yu, *J. Mater. Sci.* **44**, 3917–3927 (2009)
22. J. Xiang, Z.R. Hou, X.K. Zhang, L. Gong, Z.P. Wu, J.L. Mi, *J. Alloys Compd.* **737**, 412–420 (2018)
23. Y. Liu, F. Luo, Y. Wang, J.B. Su, W.C. Zhou, D.M. Zhu, *J. Alloys Compd.* **629**, 208–213 (2015)
24. Y.L. Zhang, X.X. Wang, M.S. Cao, *Nano Res.* **3**, 1426–1436 (2018)
25. H.L. Lv, X.H. Liang, Y. Cheng, H.Q. Zhang, Y.W. Du, A.C.S. *Appl, Mater. Interfaces* **7**, 4744–4750 (2015)

Publisher's Note Springer Nature remains neutral with regard to jurisdictional claims in published maps and institutional affiliations.